IEEE Access
Multidisciplinary | Rapid Review | Open Access Journal

SPECIAL SECTION ON GREEN INTERNET OF THINGS

Received January 22, 2020, accepted February 15, 2020, date of publication February 20, 2020, date of current version March 3, 2020.

Digital Object Identifier 10.1109/ACCESS.2020.2975424

Software Controlled Low Cost Thermoelectric Energy Harvester for Ultra-Low Power Wireless Sensor Nodes

MICHAŁ MARKIEWICZ[1,2] PIOTR DZIURDZIA[2,3], TOMASZ KONIECZNY[2], MAREK SKOMOROWSKI[1], LILIANA KOWALCZYK[2], THOMAS SKOTNICKI[2], (Fellow, IEEE), AND PASCAL URARD[4], (Member, IEEE)

[1]Faculty of Mathematics and Computer Science, Jagiellonian University, 30-348 Cracow, Poland
[2]Centre for Advanced Materials and Technologies CEZAMAT, 02-822 Warsaw, Poland
[3]Faculty of Computer Science, Electronics and Telecommunications, AGH University of Science and Technology, 30-059 Cracow, Poland
[4]STMicroelectronics, 38926 Crolles, France

Corresponding author: Michał Markiewicz (markiewicz@ii.uj.edu.pl)

This work was supported by ECSEL JU (Electronic Component Systems for European Leadership Joint Undertaking) under grant 692519–PRIME (Ultra-Low Power Technologies and Memory Architectures for IoT).

ABSTRACT General hardware architecture of an energy-harvested wireless sensor network node (EH-WSN) can be divided into power, sensing, computing and communication subsystems. Interrelation between these subsystems in combination with constrained energy supply makes design and implementation of EH-WSN a complex and challenging task. Separation of these subsystems into distinct hardware modules simplifies the design process and makes the architecture and software more generic, leading to more flexible solutions. From the other hand, tightly coupling these subsystems gives more room for optimizations at the price of increased complexity of the hardware and software. Additional engineering effort could be justified by a smaller, cheaper hardware, and more energy-efficient a wireless sensor node. The aim of this paper is to push further technical and economical boundaries related to EH-WSN by proposing a novel architecture which – by tightly coupling software and hardware of power, computing, and communication subsystems – allows the wireless sensor node to be powered by a thermoelectric generator working with about 1.5°C temperature difference while keeping the cost of all electronic components used to build such a node below 9 EUR (in volume).

INDEX TERMS Energy harvesting, thermoelectric generator, SMPS, IoT, TEG, Peltier module, boost regulator, EH-WSN, self-powered IoT node.

I. INTRODUCTION

General hardware architecture of an energy-harvesting wireless sensor network (EH-WSN) node could be divided into four subsystems: *power subsystem* (responsible for acquiring energy from a power generator, converting it into electrical energy and providing system supply voltage), *sensing subsystem* (that measures specific physical phenomena and performs analog to digital conversion), *computing subsystem* (responsible for data processing and node management) and *communication subsystem* (enabling wireless communication) [1]. The continuing trend for increasing performance, miniaturization and reducing of power consumption led to development of highly integrated System-On-Chip (SoC) hardware architectures. Some of them consist of integrated ultra-low power micro-controller units (MCUs) and radio-frequency (RF) modules, and are well suited for wireless sensing applications. Further integration of sensing subsystem and power subsystem within SoC is not common, mainly due to application specific requirements of WSN nodes. However, analog-to-digital converters (ADC) typically present on SoC are frequently used for digitalization of the electric signal from some types of sensors. In this paper we push further technical and economical boundaries related

The associate editor coordinating the review of this manuscript and approving it for publication was Nan Cheng.

to EH-WSN by proposing a novel architecture that integrates to a large extent power subsystem with a SoC of a WSN node. The paper is organized as follows:

- In section II, we describe the constraints imposed by the communication and sensing subsystems and the consequences of this for the power subsystem.
- In section III, we focus on the most fundamental component of the power subsystem of a WSN node – a power source, and more specifically, on a Peltier module as a thermoelectric generator.
- In section IV, we analyse two other elements of the power subsystem: the energy storage and the voltage converter.
- In section V, we propose an ultra-low power wireless sensor node architecture, in which power management activities are delegated to the software executed by the MCU.
- Finally, in section VI, we show the results of our experiments including tests of a thermoelectric energy harvesting wireless sensor node with power management routines executed solely by the MCU.
- In section VII, we discuss the obtained results.

II. POWER REQUIREMENTS OF WSN

The main activities of a wireless sensor node are [2]:

1) Data sampling and processing,
2) Network operations including routing, data transmission and reception.

These two activities are the most demanding in terms of power consumption. From the other hand, each WSN node could be only in one of two states:

1) Active, during which data is sampled and radio transmission is carried out, characterised by high power consumption,
2) Sleep, characterized by ultra-low power consumption.

Typically, a wireless node spends around 99% of the time in sleep mode, so overall energy budget is dominated by energy consumed in this mode [1]. Specific network architectures define the duty cycle, as well as the way the node remains synchronized with the network. Many WSNs base on the IEEE 802.15.4 standard which defines a protocol for data communication using low-data-rate, low-power, and low-complexity short-range radio frequency transmissions [3]. One of them is *GreenNet*, a radio transmission protocol that has been initially developed by STMicroelectronics and Université de Grenoble, and lately by Cezamat within PRIME (Ultra-Low Power Technologies and Memory Architectures for IoT) project [4]–[6]. To dive into the level of details required for specifying requirements for power subsystem we will use this implementation as an illustrative example of IEEE 802.15.4 wireless radio standard communication.

The GreenNet code has been enriched with debug information helping in measurements of duration and energy consumption of all activities performed by sensing, computing and communication subsystems. The summary is presented in Table 1. Power consumption waveform of the GreenNet WSN node performing network synchronization is shown in Fig. 1. The power consumption waveform of the GreenNet WSN node performing sensor data acquisition, network synchronization and data transmission is shown in Fig. 2. As expected, power consumption of the GreenNet node is significantly smaller when it is performing only network synchronization (beacon reception) than in the case when it is sensing and sending the values of sensors readouts.

TABLE 1. Power consumption during beacon reception and data transmission within one beacon cycle of the GreenNet node working with IEEE 802.15.4 beacon-enabled radio transmission protocol (input voltage: 3 V).

Activity	T [ms]	I [mA]	E [μJ]
MCU initialisation	3.5	1.42	14.91
Sensor data acquisition	4.2	5.34	67.28
Preparation to sleep	1.2	5.70	20.51
Inactivity	17.0	0.36	18.16
MCU initialisation	3.2	1.44	13.82
Preparation for beacon receiving	3.0	5.22	46.94
Radio set-up	0.7	6.23	13.08
Radio RX, sensing for a beacon	2.9	8.54	74.33
Radio RX, beacon header received	1.5	7.12	32.04
Radio RX, receiving beacon payload	1.8	8.46	45.66
Preparation to TX	1.4	6.76	28.41
Radio TX, sending data package	4.0	11.56	138.72
Radio RX, waiting for ACK	1.4	8.00	33.60
Radio off, preparation to sleep	1.3	5.70	22.21
Total	47.1	–	569.69

FIGURE 1. Power consumption profile of radio communication where there is no sensor data transmission – only beacon reception (measured as voltage drop over 5 Ω shunt resistor, input voltage: 3 V).

The IEEE 802.15.4 defines low-complexity and low-cost Reduced Function Devices (RFD) and more advanced Full Function Devices (FFD) with routing capabilities. The protocol defines beacon-enabled mode which is critical for power saving features of WSN nodes [1]. This mode is configured by two parameters BO (beacon order) and SO (superframe order), $0 \leq SO \leq BO \leq 14$. Interval between beacons is defined by equation:

$$BI = 2^{BO} \cdot t_{bsf} \tag{1}$$

For a radio symbol lasting $t_{symbol} = 16$ μs in the 2.4 GHz frequency band, and duration of the base superframe equals

FIGURE 2. Power consumption profile of radio communication where sensor data is transmitted to the router (measured as voltage drop over 5 Ω shunt resistor, input voltage: 3 V). Initially the node wakes up just before expected arrival of the beacon. Then it performs beacon reception, data transmission and goes back to a sleep mode.

TABLE 2. Energy consumption for different values of BO parameter of IEEE 802.15.4-compatible GreenNet WSN node. Energy spent on transmission is equal to the value given in Table 1. We assume that he power consumption during sleep time is equal to 3.58 μA.

BO	BI [s]	E_{sleep} [μJ]	P_{avg} [μW]	I_{avg} [μA]
0	0.02	0.00	37 089	12 363.06
1	0.03	0.00	18 545	6 181.53
2	0.06	0.00	9 275	3 091.60
3	0.12	0.00	4 643	1 547.59
4	0.25	0.00	2 327	775.59
5	0.49	0.00	1 169	389.58
6	0.98	0.01	590	196.58
7	1.97	0.02	300	100.08
8	3.93	0.04	155	51.83
9	7.86	0.08	83	27.71
10	15.73	0.17	47	15.64
11	31.46	0.34	29	9.61
12	62.91	0.68	20	6.60
13	125.83	1.35	15	5.09
14	251.66	2.70	13	4.33

to 960 symbols, we obtain $t_{bsf} = 960 \cdot t_s = 15.36$ ms. To manage the communication, FFD should to be active for:

$$SD = 2^{SO} \cdot t_{bsf} \tag{2}$$

Minimal activity time of a RFD in a single cycle is the sum of time for beacon reception and transmission of data from sensors. Without collision with other WSN nodes (which requires retransmission), energy consumed during this activity is about 570 μJ as shown in Table 1. The frequency of this activity depends on BO parameter. For $BO = 0$ energy for transmission is spent every 15.36 ms for $BO = 1$ – for every 30.72 ms, and so on. For larger BI, dominating component in energy consumption equation is not transmission but energy spent during sleep. The summary of energy expenses of a RFD as a function of BO parameter is presented in Table 2.

To summarise, as BO parameter is getting bigger, energy consumed by a RFD during sleep mode prevails in total energy budget. A FFD power budget is more complex to analyse, because not only additional SI parameter has to be taken into consideration but also network topology, support of guaranteed time slots (GTS) and other factors. Having power requirements of a RFD, we can proceed to the properties of the power source of an EH-WSN node.

III. THERMAL ENERGY HARVESTING FOR WSN

The main advantage of thermal energy harvesting for WSN node applications is its abundance in various environments, especially in a form of waste heat produced by machines [7]. In comparison to the mechanical energy sources, like vibrations, it is much more reliable as it does not require any moving parts [8]–[10]. Its relatively low power conversion efficiency (about 10%) could not match photovoltaic energy harvesters, but is able to provide stable source of energy in dark indoor industrial environments. Thermal energy could be converted into electricity by a thermoelectric generator, which principle of operation is described in the next subsection.

A. ELECTROTHERMAL MODEL OF A PELTIER MODULE

Operation of a thermoelectric module (TEG) could be described by five phenomena: Seebeck, Peltier, Thomson, Joule effects and thermal conductivity of materials [11]. The most important – from the energy harvesting point of view – is Seebeck effect, that expresses induced voltage V_S as a function of temperature difference across junction of two different materials:

$$V_S = S(T_h - T_c) \tag{3}$$

Symbol S in this equation denotes the Seebeck coefficient, i.e. the magnitude of this effect. For small changes in temperature it could be approximated by $S \approx \frac{\Delta V}{\Delta T}$.

From characteristics of thermoelectric generators [12]–[14], we have other formulas describing power balance of a working TEG:

$$Q_c = SIT_c - 0.5 \cdot RI^2 - K(T_h - T_c) \tag{4}$$

$$Q_h = SIT_h + 0.5 \cdot RI^2 - K(T_h - T_c) \tag{5}$$

$$P = Q_h - Q_c = SI(T_h - T_c) + RI^2 \tag{6}$$

$$V = \frac{P}{I} = S(T_h - T_c) + RI, \tag{7}$$

where Q_c denotes amount of heat absorbed at the cold side, Q_h – amount of heat pumped over the TEG to the hot side, P – electrical power delivered or received from/to the TEG, I – electrical current flowing through the TEG, V – voltage over TEG's terminals, S – Seebeck coefficient, K – Thomson coefficient. The value of internal resistance R can be derived from equation (7), by making the temperature of both sides the same: $T_h = T_c \implies \Delta T = 0$. The value of Seebeck coefficient can be obtained from equation (4) for $\Delta T = 0$. The value of thermal conductivity coefficient K can be derived from equation (4), assuming that no heat is absorbed at the cold side, i.e. $Q_c = 0$. This leads to formulas for the three most important parameters which characterize TEG as an energy harvesting power source:

$$R = \frac{V}{I}\Big|_{\Delta T=0} \tag{8}$$

$$S = \left.\frac{Q_c + 0.5RI^2}{IT_c}\right|_{\Delta T=0} \tag{9}$$

$$K = \left.\frac{SIT_c - 0.5RI^2}{T_h - T_c}\right|_{Q_c=0} \tag{10}$$

B. SELECTION OF A TEG MODULE

Commercially available Peltier modules cost between several EUR and several hundreds EUR as shown in Table 3. The best candidate should be able to provide enough energy to power a RFD WSN node in scenarios where energy harvesting is performed with temperature difference of a few degrees of Celsius (e.g. by being attached to an enclosure of a working machine that dissipates some heat). Having in mind that communication protocol that we are using can be parametrized – as shown in the previous section – the actual power consumption of a WSN node can be adjusted according to the performance of the power source. In the following sections we show how to make this adjustment, to enable usage of the cheapest Peltier module available on the market – TEC1-12706. According to Digi-Key, Mouser and Botland parts distributors there are several manufacturers that offer this model – some of them even for 2.85 EUR.

C. SIMULATIONS OF THE TEG PERFORMANCE

From performance curves shown in the data sheet of TEC1-12706 and equations (8)-(10) we can estimate the values of $R = 2.76\ \Omega$, $S = 36.87$ mV/K, and $K = 333$ mW/K. It means that the open circuit voltage for the temperature difference of a few degrees of Celsius is somewhere between one and two hundreds millivolts. Such a low voltage is not sufficient to directly power any MCU. Determining parameters of the power source is then critical for specifying requirements of the voltage converter.

To learn how power output of the selected TEG depends on the electrical load, and temperature difference between hot and cold side, we performed a series of simulations. As a starting point we used an equivalent electrothermal circuit presented in Fig. 3. Using LTSpice simulator with a customized model of a TEG from [11], we observed how changes in the temperature of cold and hot side influence open circuit voltage. The results are presented in Fig. 4. We can see that for small changes in temperature, plots are indeed linear, which means that we can treat Seebeck coefficient in the given temperature range as a constant.

The second set of simulations is about investigating TEG behaviour under load. The equivalent electrothermal circuit used in LTSpice is presented in Fig. 5. The results presenting output voltage V_{OUT} as a function of load I_L for different ΔT are shown in Fig. 6. From the plot we can read the internal resistance of the TEG, which is equal to the slope of the plots. Having the output voltage as a function of current load we can also compute output power – as shown in Fig. 7.

From the simulations we learned, that for temperature difference of 5°C between TEG's sides, we have approximately 190 mV open circuit voltage, and the load up to 30 mA does not cause the output voltage to drop of below 100 mV. This

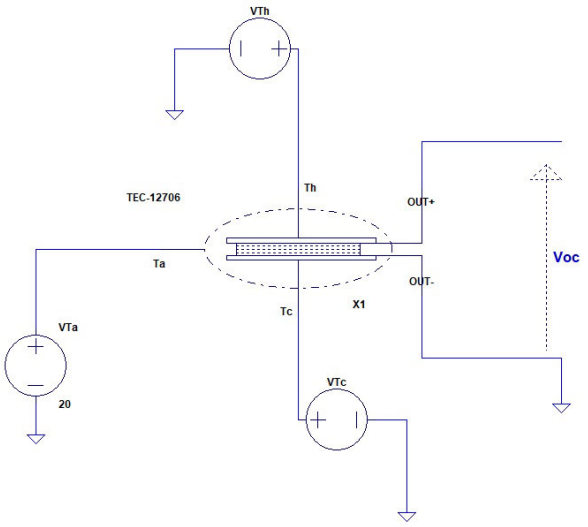

FIGURE 3. The equivalent electrothermal circuit of TEC1-12706 Peltier module used in LTSpice simulations. Ambient temperature T_a, temperature of the cold side T_c and the hot side T_h are controlled by functions V_{T_a}, V_{T_c}, and V_{T_h} respectively, according to a electro-thermal analogy.

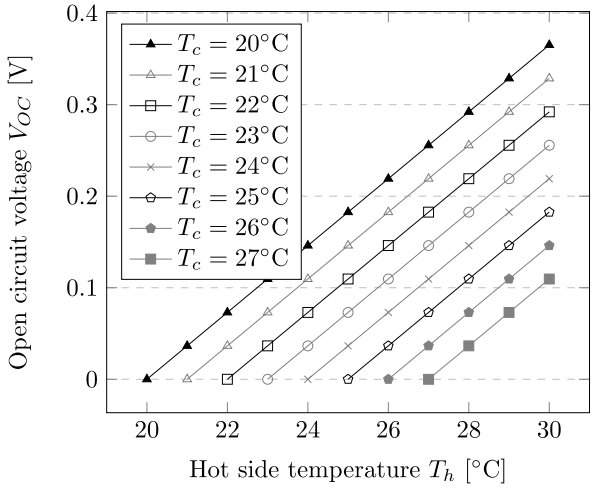

FIGURE 4. Relationship between open circuit voltage of the TEC1-12706 Peltier module and the temperature difference between its cold and hot side. For temperature difference of 5°C across TEG's sides, we have approximately 190 mV output voltage.

information will be very helpful in the selection of the power management module, which is described in the next section.

IV. ENERGY STORAGE AND VOLTAGE CONVERTER

The storage element for harvested energy must have capacity and internal resistance at levels sufficient to handle power peaks occurring during radio transmission. The other factors that have to be taken into account in selection of the energy storage are: charging and discharging characteristics, self discharge rate, cycling stability, and price. Energy management subsystem of a WSN node typically store harvested energy in either a rechargeable battery or a super-capacitor [15]. Their advantages and disadvantages are briefly presented

TABLE 3. Comparison of parameter and prices of selected Peltier modules. Unit prices for volume up to 100 pieces according to online catalogue of Digi-Key electronic components distributor (accessed January 4th, 2020).

Model	Manufacturer	Dimensions [mm]	I_{MAX} [A]	U_{MAX} [V]	Q_{MAX} [W]	R [Ω]	Unit price [EUR]
TEC1-12706	MikroElektronika	40×40×4.0	6.4	14.4	50.0 [@25°C]	1.98	4.62
430856-500	Laird Thermal Systems, Inc.	40×40×3.3	15.4	25.0	236.6 [@25°C]	1.37	57.04
CP185039	CUI Devices	50×50×3.9	18.0	15.4	157.0 [@27°C]	0.66	50.92
LCC12-10-16LS	Marlow Industries, Inc.	40×40×3.84	8.9	14.7	85.0 [@27°C]	1.32	215.87
CP90626257	CUI Devices	62×62×5.70	9.0	15.4	79.0 [@27°C]	1.31	84.46
TEC-30-40-127	Wakefield-Vette	30×30×4.0	2.5	15.4	21.4 [@25°C]	5.38	9.88
430857-501	Laird Thermal Systems, Inc.	52×52×3.3	15.4	36.0	340.6 [@25°C]	1.97	102.52

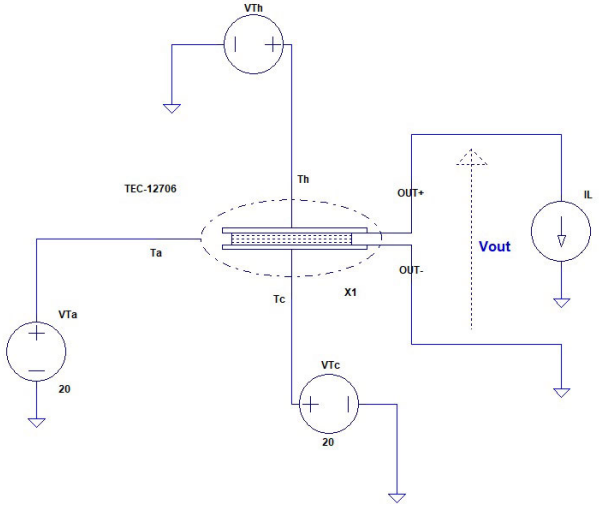

FIGURE 5. The equivalent electrothermal circuit of TEC1-12706 Peltier module used in LTSpice simulations now with load connected to the output terminals. Ambient temperature T_a, temperature of the cold side T_c and the hot side T_h are controlled by functions V_{T_a}, V_{T_c}, and V_{T_h} respectively. The load is controlled by I_L.

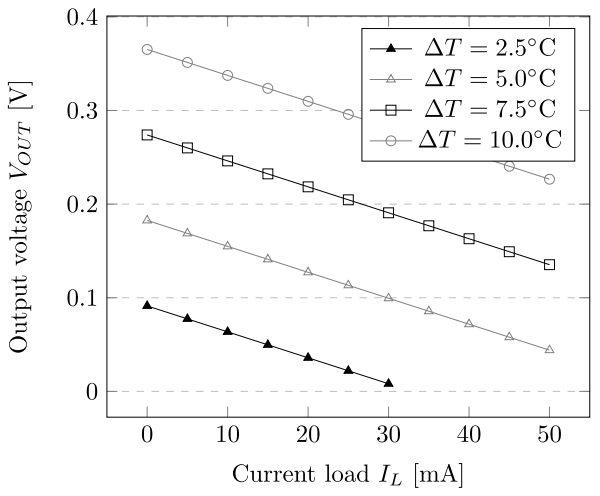

FIGURE 6. Relationship between output voltage of the TEC1-12706 Peltier module and the temperature difference between its cold and hot sides ΔT, and load current. For $\Delta T = 5°C$ (marked by grey triangles) this TEG is capable of providing load current up to 30 mA while maintaining output voltage above 100 mV.

in Table 4. A rechargeable battery has this advantage over supercapacitor, that it keeps the charge much longer. It is critical feature in industrial applications, where a EH-WSN

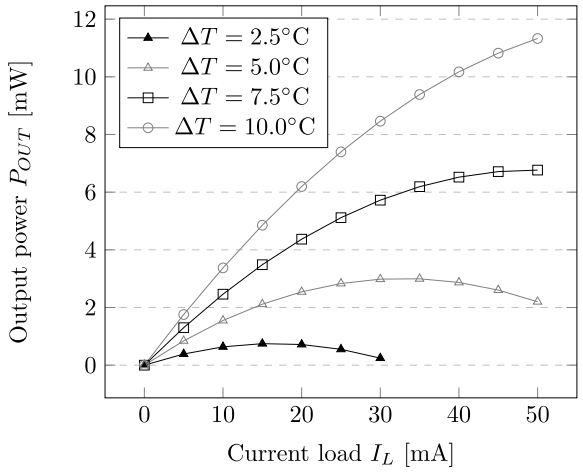

FIGURE 7. Output power in function of the current load at different temperature differences between TEG's sides ΔT. Smart power management module of a WSN node could employ maximum power point tracking algorithm (MPPT) to find the optimal load to maximize power extraction.

TABLE 4. Comaparison of selected parameters of rechargeable batteries and super-capacitors after [15].

Parameter	Rechargeable batteries	Super-capacitors
Charge/discharge efficiency	Low	High
Self discharge rate	Low	High
Energy density	High	Low
Power density	Low	High
Charging circuit complexity	High	Low
Price vs. capacity	Low	High

node could be cut off for a while from the source of thermal energy. For that reason we decided to use a rechargeable battery instead of a super-capacitor. We selected VL-2020 vanadium-lithium battery which has nominal voltage of 3 V, internal resistance of 30 Ω, and nominal capacity of 20 mAh (2.5 V cut off voltage).

The energy acquired from a TEG cannot be directly transferred to the selected energy storage. The voltage has to be increased, and the charging process has to be supervised, to avoid overcharging. Hardware architecture of a typical WSN node provides a specialized circuit – often an integrated circuit – that takes care of those activities. This circuit is called power management module, voltage converter, or charge controller, and might also perform additional tasks

like preventing the battery form deep discharging. We will discuss its functionalities in the next subsection.

A. POWER MANAGEMENT MODULE

Ultra low power charging regulators suitable for EH-WSN applications most often contain a DC/DC converter capable of stepping up input voltage. Usually it is a boost converter with an embedded switching transistor. Thresholds controlling module behaviour (e.g. cut off voltage, battery overcharging protection, battery discharging protection) are almost always set up by resistor dividers that are connected to internal analog comparators. Some modules offer extra functionalities like maximum power point tracking (MPPT) or low dropout regulators which deliver 1.8 V or 3.3 V output voltage for the MCU. The most important parameters of power management module are: quiescent current, minimum input voltage for cold start (V_{COLD}), minimum input voltage (V_{IN}), conversion efficiency and price.

From dozens of commercially available ultra-low power boost converters with battery management for energy harvesting applications, we selected three for further analysis: ADP5090, SPV1050 and LTC3108. Comparison of their features is presented in Table 5.

TABLE 5. Comparison of selected power management modules suitable to work with a thermoelectric energy harvester.

Parameter	ADP5090	SPV1050	LTC3108
Minimum input voltage for cold-start [mV]	380	550	20
Input voltage operation range [V]	0.1-3.3	0.15-18	0.02-0.5
Battery terminal charging threshold [V]	2.2-5.2	2.2-5.3	5.25
Leakage current at BAT pin [nA]	15	800	100
Leakage current at BAT pin V_{SYS}=0V [nA]	0.5	1	-
Standby current [μA]	0.8	1	6
Efficiency @ V_{IN}=0.02V [%]	-	-	35
Efficiency @ V_{IN}=0.1V [%]	40	-	25
Efficiency @ V_{IN}=1V [%]	85	85	-
Cost @ 1 unit [EUR]	4.9	2.8	6.3
Cost in volume (quantity) [EUR]	2.5 (1.5k)	1.3 (4k)	3.3 (2.5k)

SPV1050 has more functionalities in comparison to ADP5090 and LTC3108. Furthermore, it may operate in buck as well as in boost mode, and it is the best choice in terms of cost. The main drawback is its relatively high leakage current (0.8 μA). Both LTC3108 and ADP5090 have lower input voltage than SPV1050, so they are more suitable for our scenario (for $\Delta T = 5°C$, the selected TEG gives approximately 190 mV). LTC3108 has excellent cold start voltage – only 20 mV. But unfortunately it requires an external step-up transformer connected to a TEG, which significantly increases the cost. ADP5090 module is not as good as LTC3108 in terms of input voltage parameters, as it has 100 mV minimum input voltage and 380 mV cold start voltage (equivalent of $\Delta T = 10°C$). Moreover, it is also relatively expensive.

For a reference we built a EH-WSN node with ADP5090 and tested it with the selected TEG as a power source. This kind of solution – with separated power management module – without a doubt has important advantages including clean, well structured hardware architecture, very low quiescent current, high reliability and additional features like discharging protection that cuts of power supply for the MCU and all peripherals to prevent battery damage.

In the next section we will propose a novel power management architecture, and show what benefits gives resigation from a dedicated power management module.

V. A NOVEL SOFTWARE CONTROLLED LOW COST ENERGY HARVESTER

Block diagrams of power management modules described in the previous section have many elements in common. All of them contain one or more analogue comparators, internal voltage reference, DC/DC converter, and control logic. The same components can be also found in various SoC, including those with integrated IEEE 802.15.4 RF like STM32WB55 or NXP MKW41Z. Pushing downwards the cost of a WSN node with a thermoelectric energy harvester, it is tempting to propose an architecture that utilizes components already available in SoC to manage charging process.

This operation would simplify and minimize the bill of material (BOM) but obviously makes programming of the MCU more complex and challenging task.

A. POWER MANAGEMENT CONTROL LOOP

Moving the responsibility for the charging process to the MCU requires a dedicated piece of software (firmware). Unlike hardware implementation, where many things can be done in parallel, MCU executes instructions in a sequence. The control program can be presented in a form of infinite loop with the following steps:

- Measure the input voltage of the TEG,
- If the voltage across the TEG is too low then switch to a deep sleep for a while (after wake up restart the loop),
- Otherwise, measure the battery voltage,
- If the battery voltage is smaller than the maximum allowed level then start DC/DC conversion,
- Perform normal WSN operations as long as the energy budget is balanced.

Voltage measurements can be made using analog to digital converters (ADCs) commonly present in SoCs. Duration of the sleep time can be controlled from the MCU by internal timers. However, performing DC/DC conversion by the MCU with quiescent current at micro-ampere level is the biggest challenge.

B. VOLTAGE CONVERTER CIRCUIT

To step up the input voltage we used a boost converter topology [16] as shown in schematics in Fig. 8. The output signal from the MCU is connected to the gate of the switching transistor Q1. Turning on and off Q1 causes current flow through L1. The inductor temporarily stores energy in its magnetic field, and releases it through D1 to capacitor C2 and battery B1. The MCU cyclically measures battery voltage to prevent overcharging.

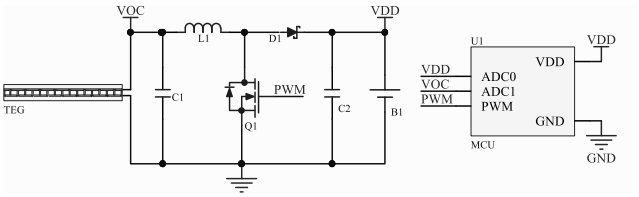

FIGURE 8. Simplified schematics of DC/DC boost converter controlled by a MCU. If V_{OC} measured by the MCU is below a threshold that guarantees battery charging during WSN operation, then the MCU goes back to a deep sleep mode just after measurement. Otherwise, the MCU starts generation of PWM that switches Q1 transistor and charges the battery.

C. POWER MANAGEMENT ALGORITHM

The program, that controls power management process, implemented on NXP MKW41Z SoC is presented as Algorithm 1.

Algorithm 1 Power Management Algorithm

1: $V_{OC} \leftarrow getTEGOpenCircuitVoltage()$
2: $V_{BAT} \leftarrow getBatteryVoltage()$
3: **if** $V_{OC} > V_{OC_{MIN}}$ **and** $V_{BAT} < V_{BAT_{MAX}}$ **then**
4: Start PWM generator at low leakage mode
5: **end if**
6: **if** $V_{BAT} > V_{BAT_{MAX}}$ **then**
7: Stop PWM
8: **end if**
9: **if** $V_{OC} - V_F > V_{BAT}$ **and** $V_{OC} < V_{BAT_{MAX}}$ **then**
10: Switch OFF Q1 to directly charge the battery
11: **end if**
12: **if** $V_{OC} - V_F > V_{BAT_{MAX}}$ **then**
13: Switch ON Q1 to save the battery
14: **end if**
15: **if** $V_{OC} > V_{OC_{RADIO}}$ and $V_{BAT} > V_{BAT_{MIN}}$ **then**
16: Normal WSN activity (turn on sensors and the radio)
17: **end if**
18: Sleep()

At the beginning, when the MCU wakes up, it measures the TEG voltage and battery voltage (lines 1-2). If the TEG voltage is greater than $V_{OC_{MIN}} = 0.04$ V, and the battery voltage is smaller than $V_{BAT_{MAX}} = 3.4$ V, then the MCU starts switching the transistor Q1, initiating charging process of the battery. If the battery voltage is greater than $V_{BAT_{MAX}}$, then transistor switching is suspended to prevent battery overcharging (line 7). If the TEG voltage decreased by the voltage drop $V_F = 0.375\ V$ over the Schottky diode D1 is greater than the battery voltage, then the transistor Q1 is turned on, so the battery could be directly charged from the TEG (line 10). If the TEG voltage minus the voltage drop over D1 diode exceeds $V_{BAT_{MAX}}$, then the transistor Q1 is turned on to protect the battery (in practical applications this case should not occur). Finally, if the TEG voltage is greater than $V_{OC_{RADIO}} = 0.18$ V, then power budget of a EH-WSN node is balanced, so normal radio activity could be resumed (line 16). Finally, the MCU sets up internal wake up timer, and goes into an ultra-low power sleep mode (line 18). All threshold voltages have been set according to the results obtained from experiments described in the next section.

TABLE 6. List of electronic parts of a low cost TEH-WSN node with a software controlled power management module. Netto prices of electronic components are given for quantities above one thousand pieces (except TEG, for which price is given for a single piece). Prices according to Digikey, Farnell, Botland and TME electronic parts distributors.

Part	Model	Price [EUR]
SoC with IEEE 802.15.4 RF	MKW21Z256VHT	2.80
Thermoelectric generator	TEC1-12706	2.85
Rechargeable Battery	VL-2020/F2N	2.04
Transistor (N-MOSFET)	AO3400	0.05
Schottky diode	MBR0530	0.04
Inductor	330 μH, <1.5 Ω	0.09
Capacitors (min. 2x)	SMD, Low ESR, 16 V	0.11
Other	Crystal, balun, resistors	1.00
Total		8.98

D. LOW POWER MODES

The proposed power management architecture cannot compete in terms of quiescent current with dedicated power management chips without a special stop modes offered by some ultra-low power microcontrollers. In a very-low-power stop mode (VLPS) current drawn by the MCU used for tests was only 3.58 μA (buck mode operation for 3 V input at 25°C) [17]. Other low power modes, such as very-low-leakage stop mode (VLLSx), allow decreasing the current down to 0.46 μA (buck mode operation for 3 V input at 25°C) [17]. These low power modes are characterized by significant reduction of MCU functionalities, but fortunately still allow some operations on GPIOs, including gating off selected peripheral clocks. The clock that we used for driving Q1 switching transistor of DC/DC boost converter has a frequency of only 1 kHz. It was operational in all power modes up to VLLS1. This clock source – called LPO (low-power oscillator) – is a part of the internal power management controller (PMC) of the selected SoC [18].

E. IMPLEMENTATION

Table 6 contains a list of parts required to build a low cost thermoelectric energy harvesting wireless sensor node (TEH-WSN). The cost of all electronic components – if purchased in volume – is about 9 EUR. For prototyping, instead of MKW21Z256VHT SoC (2.68 EUR @1k pcs.), we used Rigado R41Z-TA (6.85 EUR @1k) module that contains MKW41Z512VHT (3.25 EUR @1k), 32 MHz crystal oscillator, balun, and some other components. It increases the cost of electronic components used in the prototype to around 12 EUR. Switching to a different RF SoC with more powerful core (ARM Cortex M4) and lower power consumption in low leakage modes like STM32WB55 (2.97 EUR @ 1k, 600 nA in standby mode with RTC and 32 KB RAM retention [19]) should not greatly impact the total price.

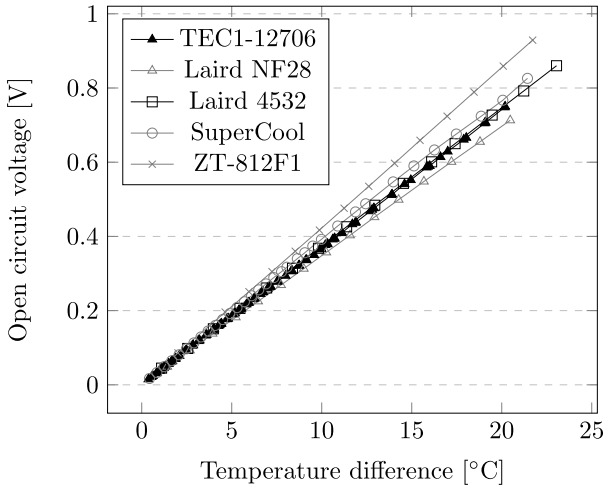

FIGURE 9. Measured open circuit voltages of several different Peltier modules as a function of temperature difference ΔT. For low values of ΔT, all tested modules behave similarly.

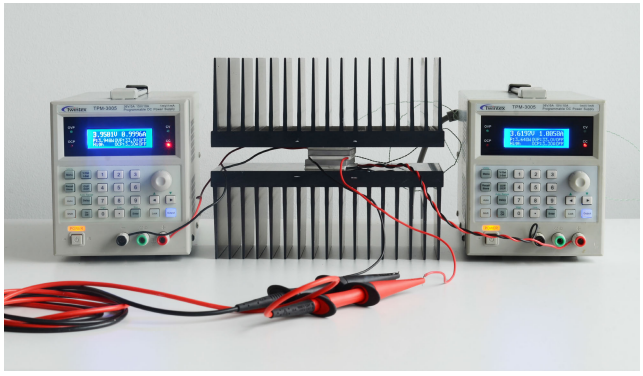

FIGURE 10. Each TEC1-12706 Peltier module is connected to a separate Twintex TPM-3005 programmable power supply. Heat and cold from two auxiliary Peltier modules are dissipated by large heat sinks. Between these two modules there is a third one working as a thermoelectric generator. Thermocouples placed between modules are connected to the Pico TC-08 thermocouple data logger. Open circuit voltage is measured by the PicoLog 1216 data logger.

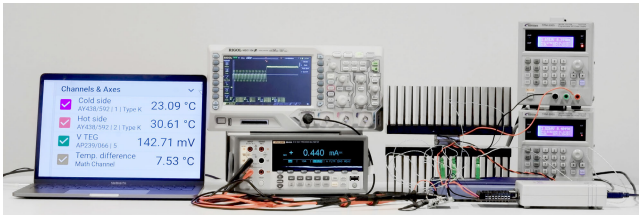

FIGURE 11. Testbed for measurements of efficiency of thermoelectric generator connected to the power management module under constant load. On the left hand side, a computer with a software that shows values of thermocouples and voltage of a TEG; next to it Rigol MSO1105 oscilloscope connected to the TEG, and displaying a TEG voltage in time; under it Fluke 8846A ammeter displaying current flowing into battery; next to them stack of heat sinks and Peltier modules connected to two Twintex TPM-3005 programmable power supplies. Thermocouples are connected to the Pico TC-08 data logger and TEG voltage is measured by the PicoLog 1216 Data Logger.

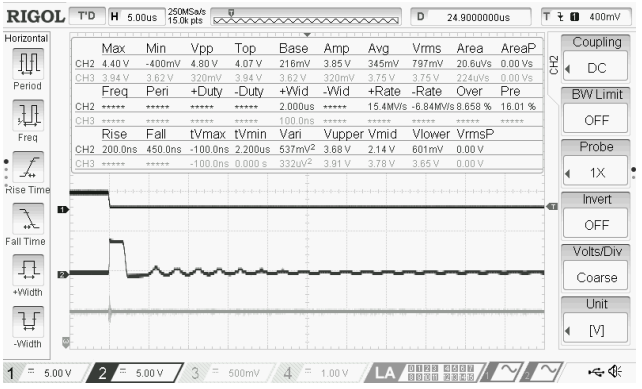

FIGURE 12. Waveforms related to the MCU-controlled DC/DC boost converter working in discontinuous mode. The first probe is connected to the gate of the transistor Q1 (designators according to the schematics shown in Fig. 8). The second probe is connected to the drain of Q1. After driving the gate low, the voltage at the inductor L1 is increasing very rapidly and goes through the Schottky diode D1 to the capacitor C2. The third probe is connected to C2. This experiment was conducted without the battery B1, so the energy that keeps the MCU working comes only from the capacitor C2 (2200 μF, 16 V).

VI. EXPERIMENTS AND RESULTS

To verify the concept of the energy harvesting architecture described in the previous section we conducted a series of experiments. At first we verified the correctness of open circuit voltage estimation calculated by LT Spice for different Peltier modules, as shown in Fig. 9. Tests confirmed results obtained from simulations. To ensure stability of test conditions – including proper temperature on both sides – tested modules were put between a pair of other Peltier modules which were connected to a pair of laboratory power supplies. Current flowing through them generated a temperature difference between their inner sides. Heat and cold from their outer sides were dissipated by large heat sinks as shown in Fig. 10.

The second set of experiments was about verification of the idea of having net power gain with a DC/DC boost converter driven by the MCU at low power mode. Initially the switching transistor has been driven by an arbitrary function generator to find the best configuration of inductor value and duty cycle of pulse-width modulated signal. The same experiments have been conducted using LTSpice simulations. We used a testbed with a Peltier module as shown on Fig. 11, and more convenient laboratory power supply with a resistor connected in series that mimics internal resistance of a Peltier module.

The experiments ended up with the selection of AO3400 N-channel MOSFET (with $V_{GS} \leq 1.45\ V$) as a switching transistor, PWM signal with 50% duty cycle, frequency of 1 kHz, and an inductor of 330 μH and series resistance below 1.5 Ω. An inductor with significantly lower resistance (440 Ω) offered much better performance, but because it was almost seven times more expensive, we used the cheaper one. Fig. 12 shows waveforms of charging circuit with the final configuration. More power could be drawn from a TEG with higher duty cycle, but generation of a simple, symmetrical, low frequency signal was possible to obtain using the selected SoC working in a low power mode.

TABLE 7. Energy balance for different ΔT. The load resistor R_{LOAD} is connected in parallel to the MCU to mimic the energy consumed by the radio activity and some additional sensors. Each row in this table should be read as following: for example at $\Delta T = 5°C$, the open circuit voltage of the TEG is about 180 mV. For this input voltage, the circuit shown in Fig. 8 has a RMS voltage of 3.09 V. With resistive load $R_{LOAD} = 327\ k\Omega$ connected in parallel to the MCU, the average power dissipated by the R_{LOAD} resistor is equal to 1mW (because of current of 327 μA passing through it). This amount of power corresponds to the situation when the IEEE 802.15.4 beacon-enabled radio is working with BO≥6 (according to the Table 2 for BO = 6 the device is transmitting every second, and consumes in average 590 μW – less than 1012 μW dissipated by the R_{LOAD} resistor).

ΔT [°C]	V_{OC} [V]	V_{RMS} [V]	R_{LOAD} [kΩ]	I_{avg} [μA]	P_{avg} [μW]	BO
1.00	36	3.09	2104	1.47	4.54	–
1.28	46	3.09	702	4.40	13.60	14
1.50	54	3.10	250	12.42	38.52	10
2.00	72	3.11	88	35.54	110.54	8
2.50	90	3.05	45	68.00	207.41	8
3.00	108	3.10	29	106.68	330.70	7
3.50	126	3.09	20	152.97	472.68	7
4.00	144	3.09	17	184.48	570.04	7
4.50	162	3.09	12	259.45	801.69	6
5.00	180	3.09	9	327.68	1012.52	6
5.50	198	3.09	8	406.04	1254.68	5
6.00	216	3.09	6	484.33	1496.57	5

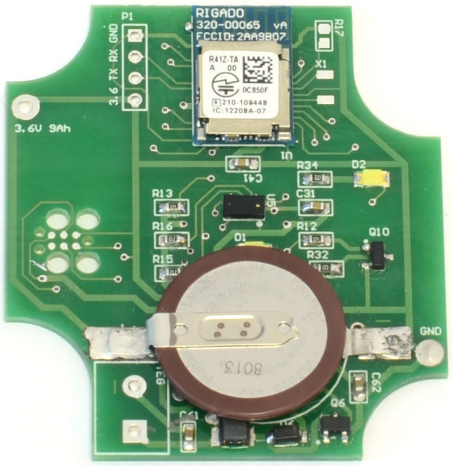

FIGURE 13. The wireless sensor node that could be powered either from a thermoelectric generator (connector located at bottom left) working with VL-2020 lithium-vanadium rechargeable battery, or from a non-rechargeable lithium battery. The node contains of Rigado R41Z module with SoC ARM Cortex-M0+ MCU with 512 KB Flash and 128 KB SRAM, and IEEE 802.15.4 RF (at the top), VL53L0X time of flight sensor (in the middle), and MCU-controlled DC/DC boost converter (at the bottom).

The aim of the third set of experiments was to measure the energy balance of the EH-WSN node. We connected a potentiometer R_{LOAD} in parallel to the MCU to mimic the average energy consumption of the radio and node sensors. Greater ΔT means greater open circuit voltage of the TEG. By altering the resistance of R_{LOAD} we were able to find the maximum average power that could be consumed by the radio activity and sensors. The results are presented in Table 7. At $\Delta T = 1°C$, the MCU can only charge the battery because the energy supply is not sufficient to establish radio communication. At $\Delta T = 1.28°C$ the radio can be activated with about 4 minutes 11 seconds time interval between sending messages. As ΔT increases, the amount of harvested energy allows to support not only more frequent communication but also external sensors. For increasing input voltages, we observed that the DC/DC converter maximum instantaneous output voltage was getting close to the maximum absolute value of the MCU. To minimize the impact of voltage spikes to the MCU and the battery, a low-pass filter is recommended between the capacitor C2 and the battery B1.

Finally, we tested the wireless sensor node as a fully functional element of a wireless sensor network. We used WSN node with a sample sensor – STMicroelectronics VL53L0X Time-of-Flight (ToF) laser-ranging module, which can measure absolute distances up to 2 m, and Rigado R41Z module with MKW41Z512 SoC as is shown in Fig. 13.

The experiments proved that the proposed solution works as designed.

TABLE 8. Comparison of two EH-WSN nodes architectures: with a dedicated power management chip and with software controlled power management.

Parameter	Dedicated chip	Software supervision
Reliability	Higher	Lower
Complexity	Lower	Higher
Flexibility	Lower	Higher
Battery protection	Higher	Lower
Hardware cost	Higher	Lower

VII. CONCLUSION AND FUTURE WORK

The architecture of the EH-WSN node described in this paper is the answer to a challenge formulated in PRIME project made within Electronic Components and Systems for European Leadership JU Programme. The goal was to propose a low cost wireless sensor node (< 9 EUR target), communicating wirelessly using one of the IEEE transmission standards, fully autonomous with thermoelectric energy harvester working with temperature difference $\leq 5°C$. It was intended to push the firmware optimization to the extreme and to enforce a tight link between hardware and software. In this sense the proposed architecture achieved the goal. We hope, that it would be also useful in exploration of software and hardware architectures of WSN, and will contribute to spreading of autonomous Internet of Things devices.

In Table 8 we summarized advantages and disadvantages of the proposed software controlled power management architecture in relation to the architecture with a dedicated power management chip.

The most fundamental drawback of the proposed solution is that the program executed by the MCU has to be very carefully written. A potential consequence of a software bug that causes malfunction of the power management control loop is permanent destruction of the battery. Another downside is that once the rechargeable battery is drained (which might happen when a node is stored for too long without access

to thermal energy), then it is no longer possible to start the device without charging the battery from an external source.

The main advantage of the proposed solutions is that it helps in decreasing hardware cost of a WSN node. It also takes the flexibility of power management to another level – the node could dynamically decide about voltage thresholds related to the sensor activity. In the context of industrial or wearable applications, it might offer additional functionalities. For example the node can temporarily decrease cut off voltage, to ensure that all critical data will be transmitted, when detecting an unusual condition. Similarly, it might temporarily increase overcharging protection threshold (while remaining in the safe operation area of the battery) to store more energy, that will be spend on scheduled bulk radio transmission like firmware update, or other energy intensive activities like sensor calibration.

In the future we would like to investigate possibilities of making power management process independent of user application, possibly by integrating it with an embedded real time operating system (RTOS) with a preemptive scheduler.

REFERENCES

[1] M. Kuorilehto, M. Kohvakka, J. Suhonen, P. Hamalainen, M. Hannikainen, and T. D. Hamalainen, *Ultra-Low Energy Wireless Sensor Networks in Practice: Theory, Realization and Deployment*. Hoboken, NJ, USA: Wiley, 2008.

[2] M. R. Hansen, M. K. Jakobsen, and J. Madsen, "A modelling framework for energy harvesting aware wireless sensor networks," in *Sustain. Energy Harvesting technol.*, Y. K. Tan, Ed. Rijeka, Croatia: IntechOpen, 2011, ch. 1, doi: 10.5772/26622.

[3] (2015). *IEEE 802.15.4-2015—IEEE Standard for Low-Rate Wireless Networks*. [Online]. Available: https://standards.ieee.org/standard/802_15_4-2015.html

[4] L.-O. Varga, G. Romaniello, M. Vucinic, M. Favre, A. Banciu, R. Guizzetti, C. Planat, P. Urard, M. Heusse, F. Rousseau, O. Alphand, E. Duble, and A. Duda, "GreenNet: An energy-harvesting IP-enabled wireless sensor network," *IEEE Internet Things J.*, vol. 2, no. 5, pp. 412–426, Oct. 2015.

[5] P. Urard, G. Romagnello, A. Banciu, J. C. Grasset, V. Heinrich, M. Boulemnakher, F. Todeschni, L. Damon, R. Guizzetti, L. Andre, and A. Cathelin, "A self-powered IPv6 bidirectional wireless sensor & actuator network for indoor conditions," in *Proc. Symp. VLSI Circuits (VLSI)*, Jun. 2015, pp. C100–C101.

[6] G. Romaniello, "Energy efficient protocols for harvested wireless sensor networks. (pile de protocoles pour des réseaux des capteurs avec récupération d'énergie)," Ph.D. dissertation, Dept. DBLP Comput. Sci. Bibliography, Grenoble Alpes Univ., Saint-Martin-d'Hères, France, 2015. [Online]. Available: https://tel.archives-ouvertes.fr/tel-01149450/document

[7] Y. K. Ramadass and A. P. Chandrakasan, "A battery-less thermoelectric energy harvesting interface circuit with 35 mV startup voltage," *IEEE J. Solid-State Circuits*, vol. 46, no. 1, pp. 333–341, Jan. 2011.

[8] A. D. Joseph, "Energy harvesting projects," *IEEE Pervas. Comput.*, vol. 4, no. 1, pp. 69–71, Jan. 2005.

[9] S. Beeby and N. White, *Energy Harvesting for Autonomous Systems*. Norwood, MA, USA: Artech House, 2010.

[10] S. Priya and D. J. Inman, *Energy Harvesting Technologies*. Boston, MA, USA: Springer, 2009. [Online]. Available: https://link.springer.com/content/pdf/10.1007%2F978-0-387-76464-1.pdf

[11] P. Dziurdzia, "Modelling and Simulation of Thermoelectric energy harvesting processes," *Sustainable Energy Harvesting Technologies—Past, Present and Future*, Kraków, Poland: AGH University of Science and Technology, pp. 109–116, 2011.

[12] P. Dziurdzia, P. Bratek, I. Brzozowski, W. Gelmuda, J. Ostrowski, and A. Kos, "Extraction of temperature dependent parameters for an electrothermal model of thermoelectric energy harvester," in *Proc. 23rd Int. Conf. Mixed Design Integr. Circuits Syst.*, Jun. 2016, pp. 1–5.

[13] T. Nunnally, D. Pellicone, N. Van Velson, J. Schmidt, and T. Desai, "Thermoelectric performance model development and validation for a selection and design tool," in *Proc. 14th Intersociety Conf. Therm. Thermomech. Phenomena Electron. Syst. (ITherm)*, May 2014, pp. 1404–1411.

[14] R. Buist, "Calculation of peltier device performance," *CRC Handbook Thermoelectrics*. Boca Raton, FL, USA: CRC Press, 1995, pp. 143–155.

[15] F. Akhtar and M. H. Rehmani, "Energy replenishment using renewable and traditional energy resources for sustainable wireless sensor networks: A review," *Renew. Sustain. Energy Rev.*, vol. 45, pp. 769–784, May 2015.

[16] P. Horowitz and W. Hill, *The Art of Electronics*. Cambridge, U.K.: Cambridge Univ. Press, 2015.

[17] *MKW41Z/31Z/21Z Data Sheet, NXP Semiconductors, 3 2018, Rev. 4*. Accessed: Aug. 12, 2019. [Online]. Available: https://www.nxp.com/docs/en/data-sheet/MKW41Z512.pdf

[18] *MKW41Z/31Z/21Z Reference Manual, NXP Semiconductors, 10 2010, Rev. 1*. Accessed: Aug. 12, 2019. [Online]. Available: https://www.nxp.com/webapp/Download?colCode=MKW41Z512RM

[19] *STM32WB55xx Data Sheet: Multiprotocol Wireless 32-Bit MCU Arm-Based Cortex-M4 With FPU, Bluetooth5 and 802.15.4 Radio Solution, ST Microelectronics, 2 2019, Rev. 4*. Accessed: Dec. 2, 2019. [Online]. Available: https://www.st.com/resource/en/datasheet/stm32wb55rg.pdf

MICHAŁ MARKIEWICZ received the M.Sc. degree from Jagiellonian University, Faculty of Mathematics and Computer Science, in 2006, and the Dr. Ing. degree from Bremen University, Bremen, Germany, in 2015. He is currently an Assistant Professor with the Faculty of Mathematics and Computer Science, Jagiellonian University and a Research Program Coordinator at Cezamat PW. His scientific interests include sensor networks, traffic management, and power electronics.

PIOTR DZIURDZIA received the M.Sc. and Ph.D. degrees from the AGH University of Science and Technology (AGH UST), Cracow, Poland, in 1995 and 2000, respectively. He is currently with the Department of Electronics, AGH UST and Cezamat PW. He is also working on energy harvesting applications in wireless sensor networks and modeling of electrothermal processes in thermoelectric modules.

TOMASZ KONIECZNY received the M.Sc. degree in electronics and telecommunications from the Silesian University of Technology, Gliwice, Poland, in 1994. Since 1995, he has been a Designer (the Chief Designer or the Project Manager) in research and development departments. He is currently employed as a Researcher at Cezamat PW.

MAREK SKOMOROWSKI received the Ph.D. degree in computer science from the AGH University of Science and Technology, Cracow, Poland, in 1984. He specializes in image recognition and computer simulation. He has been a Full Professor and the Director of the Computer Science and Computer Mathematics Institute, Jagiellonian University, Cracow.

THOMAS SKOTNICKI (Fellow, IEEE) received the B.Eng. and M.Sc. degrees in electronics from the Warsaw University of Technology, Warsaw, Poland, in 1979, the Ph.D. degree from the Institute of Electron Technology, Warsaw, in 1985, and the Habilitated for Directing Research degree from the Institut National Polytechnique de Grenoble, Grenoble, France, in 1993. He has been a Full Professor from Poland, since 2007. He is currently the CEO of Cezamat PW.

PASCAL URARD (Member, IEEE) received the Engineering degree from ISEN, Lille, France, in 1991. In 2000, he joined ST Crolles Central R&D, Crolles, France. In 2010, he initiated the first autonomous IPv6 wireless network for sensors and actuators (GreenNet), demonstrating bidirectional secured IPv6 communications over the air powered by energy harvesters. As an ST Fellow, he is currently working on ultralow-power and energy-efficient solutions for the IoT.